ELSEVIER

Journal of Nuclear Materials 297 (2001) 62–68

journal of nuclear materials

www.elsevier.com/locate/jnucmat

# Oxide layers of Zr–1% Nb under PWR primary circuit conditions

Gabor Nagy [a,*], Zsolt Kerner [a], Gábor Battistig [b], Anna Pintér-Csordás [a], János Balogh [a], Tamás Pajkossy [a]

[a] *Department of Physical Chemistry, KFKI Atomic Energy Research Institute, P.O. Box 49, H-1525 Budapest, Hungary*
[b] *HAS Research Institute for Technical Physics and Materials Science, P.O. Box 49, H-1525 Budapest, Hungary*

Received 23 November 2000; accepted 7 April 2001

**Abstract**

Oxide layers were grown on Zr–1% Nb under conditions simulating those in VVER-type pressurised water reactors (PWRs), viz. in borate solutions in an autoclave at 290°C. The layers were characterised by various methods: their respective thickness values were determined by weight gain measurements, Rutherford backscattering (RBS), nuclear reaction analysis (NRA) and scanning electron microscopy (SEM); the electrical properties were tested by electrochemical impedance spectroscopy. The results show that the oxide layer on Zr–1% Nb is homogeneous and somewhat thicker than that on Zircaloy-4. © 2001 Elsevier Science B.V. All rights reserved.

## 1. Introduction

Zirconium alloys are essential in nuclear reactor technology, functioning as fuel cladding, pressure tubes, fuel channels and fuel spacer grid materials. Generally speaking, the zirconium alloys performed satisfactorily in service, but there have been occasional problems including those of fuel cladding and pressure tube degradation and failure.

Recently, new expectations and trends have emerged that require extensive experimental and theoretical investigations of zirconium alloy corrosion. The prerequisites for more severe operating conditions, longer service time, higher burnups, higher pH in pressurised water reactor (PWR) coolants and other service modifications are driving the research activity in this field. Although the basic trends in corrosion behaviour seem to be understood [1], the mechanism of the processes still requires a sound basis of interpretation and prediction is still insufficiently well described [2]. The need for a more detailed understanding of zirconium alloy behaviour is obvious.

Despite the great number of experimental and theoretical results available in the literature concerning zirconium alloy behaviour in western-type PWRs and boiling water reactors (BWRs) (see e.g. [1–3] and references therein) much less information is available on the VVERs, these being Russian-type PWRs. Only recently international conferences and publications have devoted more concern to this type of nuclear reactor [4].

Several techniques are used to study the corrosion processes on zirconium alloys and to characterise the protective oxide layer of these materials. The ex situ methods (like the ones used in the present study) provide morphological and chemical composition data of the oxide layer. SEM is also routinely used for studying zirconium alloys [1]: both scanning electron microscopy (SEM) and transmission electron microscopy (TEM) are capable, both in normal and in backscattered mode, of analysing oxide topography and morphology [5]. By investigating cross-sectional samples the oxide/metal interface and the alloy texture can be visualised [6,7].

Apart from the above methods, electrochemical techniques, e.g., measurements of the open circuit potential (OCP) and electrochemical impedance spectroscopy (EIS) are widely used because they give in situ

* Corresponding author. Tel.: +36-1 392 2222; fax: +36-1 392 2299.
*E-mail address:* nagyg@sunserv.kfki.hu (G. Nagy).


PII: S0022-3115(01)00596-7

information either on the kinetics of the corrosion process or on the oxide layer thickness. Ample results are available for the various western-type PWR and BWR cladding materials, Zircaloys, measuring the thickness of the protective oxide layer and its structure (see e.g. [8–12] and references therein); less information is available, however, for the VVER cladding material, Zr–1% Nb (see e.g., [4,13]).

The aim of our work – due to this lack of relevant data – is to gain understanding of the corrosion behaviour and oxide layer growth of Zr–1% Nb along with a comparison of the most widely used zirconium alloy (Zircaloy-4) in a simulated VVER primary circuit environment. To this end, samples of the two alloys were autoclaved and, periodically, the oxide layers were characterised by weight gain measurements, SEM, RBS, NRA and electrochemical impedance spectroscopy.

## 2. Experimental

Zircaloy-4 and Zr–1% Nb tubular samples were cleaned in accordance with the ASTM G2M standard. A set of samples was placed into a PARR 4532 autoclave filled with an aqueous solution containing 0.8 g/kg boric acid, 5 mg/kg ammonium hydroxide and 5 mg/kg potassium hydroxide – these being typical concentrations of the primary circuit of a VVER. Analytical grade chemicals and ultrapure water obtained from a REWA clean water system were used. After deaeration by argon gas the samples were kept in the solution at 290°C for 2–84 days. The simplest (though not precise) method of determining oxide layer thickness is gravimetry: the samples were washed, dried and their weight was measured before and after autoclaving. From the weight gain, using the $\rho = 5.68$ g/cm$^3$ density value, the average oxide layer thickness could be calculated.

SEM (using a device of Philips SEM 505 type, working at 10 and 15 kV, respectively) was utilised to study the Zr–1% Nb tubes. Two types of samples were studied: outer surfaces and cross-sections. The latter were prepared by embedding the tubes into a two-component epoxy resin, then grinding and polishing their cross-sectional surface. A conductive carbon layer with a thickness of about 20 nm was evaporated onto the samples. A Centaurus-type backscattered detector was used to reveal the thin oxide layer on the surface of the tubes.

The thickness of the oxide layers was also measured by NRA and RBS. These measurements were carried out employing ion beams provided by our Institute's 5 MeV van de Graaff accelerator. These methods give the oxygen contents of the surface layer of 2–3 μm with a detection limit of 100–1000 ppm, depending on the depth. Ordinary RBS [14] with a proton beam hardly gives information about oxygen (since it is lighter than the other elements in the target), however, applying a 3.05 MeV $He^+$ analysing beam with a much higher cross-section value, we can extract the oxygen content of the samples from the recorded spectra.

Another possible ion beam analytical method for measuring the oxygen content of a sample is NRA [14]. The $^{16}O(d, p)^{17}O^*$ nuclear reaction at around 950 keV bombarding energy can be applied to measure the oxygen in a sample with high precision (in the range of 1000 ppm) separately from other elements. In our case 13 μm Mylar foil stopped the backscattered deuterons in front of the detector as a result of which only the reaction product protons were detected.

With both ion beam methods the integral of certain peaks is proportional to the total amount of oxygen present in the sample. To calibrate the method, i.e., to obtain the absolute amount of oxygen, a well-known reference sample had to be measured under the same experimental conditions. For this we used a thermally grown $SiO_2$ film on Si with a thickness of 56 nm (this value had earlier been determined by spectroscopic ellipsometry). We compared the peak integrals from the reference sample and the zirconium samples to enable the oxygen amounts to be extracted and, supposing a stoichiometric $ZrO_2$ surface layer with a density of 5.68 g/m$^3$, the corresponding oxide layer thickness could be calculated.

We used Solartron 1286 or Electroflex EF453 potentiostats coupled to a Solartron 1250 frequency response analyser for our electrochemical impedance spectroscopy (EIS) measurements. Typically, EIS measurements were carried out in the frequency range from 64 kHz to 0.1 Hz with ac amplitude of 5 mV. A conventional three-electrode cell was used with a large platinum foil counter electrode and a calomel reference (SCE; all the potential values are given on its scale).

Although these methods are able to provide information about the oxide layer, their capabilities do not allow us to draw conclusions about the oxidation state of the elements in the alloy. Moreover, we cannot detect changes in the alloy composition – even by using energy dispersive microanalysis we were not able to separate the niobium from the zirconium since they are neighbours in the periodic table. Information can only be obtained by surface analytical techniques such as ESCA or Auger electron spectroscopy.

## 3. Results and discussion

After autoclave treatment the Zircaloy-4 and Zr–1% Nb samples were analysed to determine the rate of corrosion from the thickness of the oxide layers formed. Weight gain, RBS, NRA, SEM and electrochemical measurements were performed.

### 3.1. RBS and NRA measurements

NRA gives information about the oxygen content of the Zr–1% Nb samples. On the spectra (Fig. 1) three proton groups appear. The peak around channel 430 corresponds to the protons from the nuclear reaction $^{12}C(d,p)^{13}C$. There is always some deposition of hydrocarbons originating from the air at the sample surface; this is why we always observe some carbon. The other two proton groups at channel 330 and channel 190 correspond to the $p_0$ and $p_1$ reaction product from $^{16}O(d,p)^{17}O^*$. The integral of these peaks is proportional to the total amount of oxygen present in the sample. The thickness was calculated by assuming that (i) the layer is considered to be homogeneous with (ii) stoichiometric $ZrO_2$ composition, thus (iii) the metal/oxide interface is two-dimensional. As we will see later these conditions are not fulfilled but they are useful for standardising and simplifying our calculations. The values are listed in Table 1.

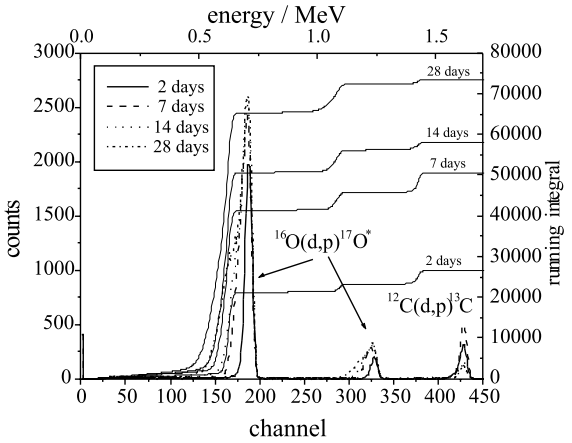


Fig. 1. NRA spectra for Zr–1% Nb samples after 2, 7, 14 and 28 days oxidation. The spectra were recorded at 950 keV bombarding deuterium energy at 150° detection angle. In front of the surface barrier detector 13 μm Mylar was used to stop the backscattered deuterium ions. The running integrals of the spectra, proportional to the oxygen content, are also shown.

RBS is not only able to provide the thickness of the oxide layer but it also gives information about the stoichiometry and homogeneity of the layer. The interpretation of RBS spectra is straightforward. Analysing the curves in Fig. 2 one can see that the stoichiometry of the oxide layer changes in the region between channels 200 and 500. The oxygen content is somewhat higher than that of the stoichiometric composition of $ZrO_2$ at the surface (at ch. 475). With increasing depth into the oxide layer the zirconium content is almost constant in the $ZrO_2$ phase. The thickness of this phase increases with the oxidation time. Further towards the bulk of the sample the oxygen content decreases, and after a certain distance from the surface the spectra show no oxygen indicating that the oxygen content is lower than the detection limit of the RBS method. The region where the oxygen content changes gradually is believed to be an α-Zr(O) phase. The thickness of this phase also increases with oxidation time. This clearly shows that the interface between the metallic zirconium alloy and the oxide is not sharp.

The oxygen content of the α-Zr(O) phase changes linearly within the layer. We chose the middle of this region as a theoretical interface between the oxide and the metal. Thus, the thickness of the oxide layer was considered as the distance between this position and the surface of the sample. Clearly, this definition is similar to that used to evaluate the NRA measurements, and it gives only an estimate of the thickness. The calculated values are listed in Table 1.

Table 1
Oxide layer thickness (in μm) of autoclave-treated samples measured by weight gain, SEM, RBS and NRA. The estimated errors are in the range of ±0.05, ±0.5, ±0.01 and ±0.01 μm, respectively

| Alloy | Time (day) | Weight gain (μm) | SEM (μm) | RBS (μm) | NRA (μm) |
|---|---|---|---|---|---|
| Zircaloy-4 | 7 | 1.00 | | 0.55 | |
| | 28 | 1.42 | | 0.58 | |
| | 56 | 1.64 | | 1.00 | |
| | 84 | 2.11 | | 0.98 | |
| Zr–1% Nb | 2 | 0.31 | 0.3 (not uniform) | 0.26 | 0.31 |
| | 7 | 1.01 | 1.0 (not uniform) | 0.70 | 0.71 |
| | 14 | 1.13 | 1.0 | 0.95 | 0.89 |
| | 28 | 1.07 | 0.9 | 0.63 | 0.72 |
| | 42 | 2.01 | 1.7 | 1.15 | 1.14 |
| | 56 | 1.19 | | 0.76 | 0.85 |
| | 70 | 1.57 | | 0.84 | 1.00 |
| | 84 | 1.95 | | 1.40 | 1.21 |

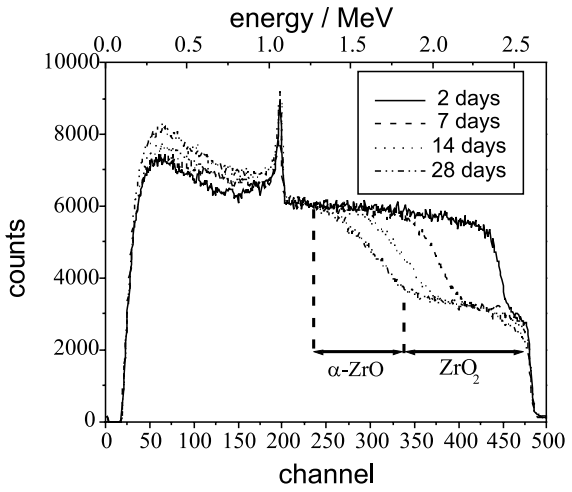


Fig. 2. RBS spectra of Zr–1% Nb samples after 2, 7, 14 and 28 days oxidation (beam: 3.05 MeV $^4$He; scattering angle: 165°). The high peak around ch. 190 stems from the oxygen in the surface layer.

### 3.2. Gravimetry and microscopy

Oxide thickness values were also estimated from weight gain measurements. For the calculations we used the usual standardising assumptions: (i) the layer is con- sidered to be homogeneous with (ii) stoichiometric $ZrO_2$ composition, thus (iii) the metal/oxide interface is two-dimensional. The thickness values are listed in Table 1.

SEM is capable of determining the thickness of the oxide layers directly from the cross-sectional images of the surface region. By analysing the SEM images (Fig. 3) one can conclude that the oxide layer is far from the uniform state on the sample with the shortest treatment time (2 days). In this case, the average thickness value is not representative of the oxide layer on the specimen. The oxide layers of samples with longer treatment times were found to be almost uniform. The thickness values are given in Table 1.

As can be seen from Table 1, we obtained layers with an average thickness of 1–2 μm during the time scale of autoclave oxidation of Zr–1% Nb and Zircaloy-4. The results suggest that the corrosion rate of the alloys is almost the same – maybe it is somewhat larger for Zr–1% Nb in this time range. This observation is in accordance with the literature data [9]. Despite the uncertainty of the gravimetric measurements being too large, the RBS results are accurate enough to allow comparison between the two types of alloys.

The thickness values of Zr–1% Nb from gravimetry and SEM are almost identical (although one should take the large uncertainty of SEM results into account), but considerably larger than those from RBS and NRA (cf. Fig. 4). These latter two methods also gave very similar results to each other. To understand the difference we should take into account that gravimetry measures the total oxygen content, whereas the detection limit of RBS and NRA is around 1000 ppm. If oxygen diffuses into the bulk alloy in small concentrations these latter two methods cannot detect the element. This may explain the 30% difference in the thickness values. In other words, 30% of the total oxygen amount can be dissolved in the metallic phase, as was often found [1,2]. Estimating roughly the thickness of the alloy phase where oxygen is dissolved with a concentration of 1000 ppm we got a value of the order of 10 μm.

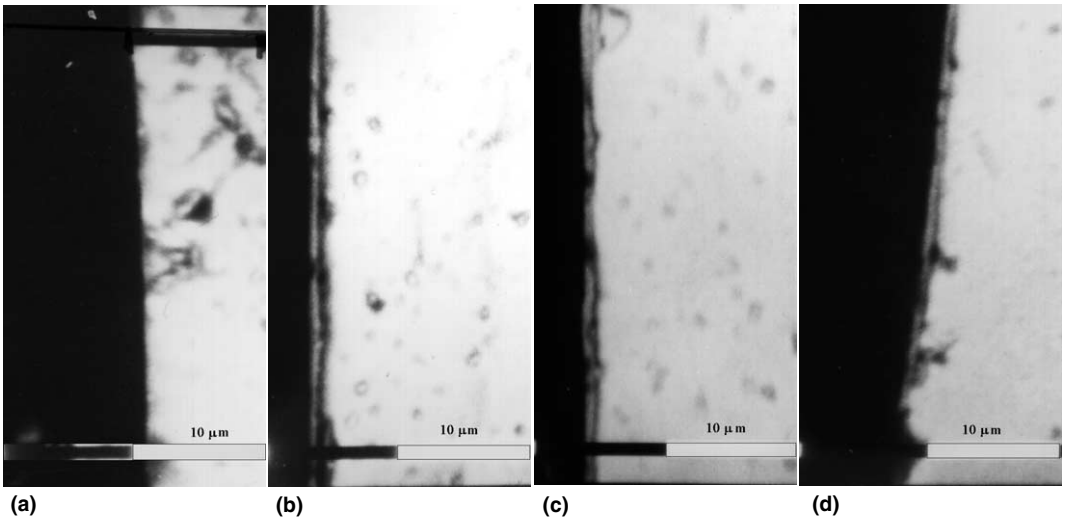


Fig. 3. Cross-sectional SEM pictures of Zr–1% Nb samples after (a) 2, (b) 7, (c) 14 and (d) 28 days oxidation (white regions – alloy, black regions – epoxy resin). In all cases, regions of 20 μm in horizontal direction are shown.

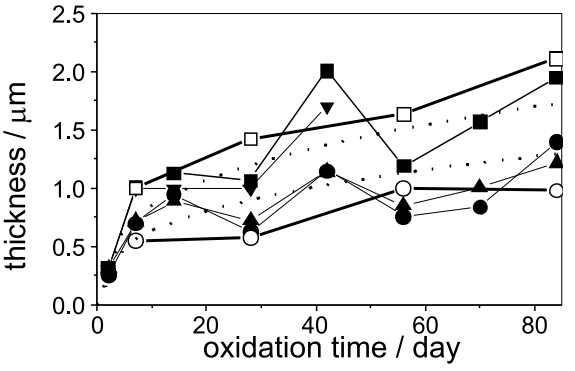


Fig. 4. Zircaloy-4 (empty symbols) and Zr–1% Nb (filled symbols) oxide layer thickness as a function of oxidation time. (squares – gravimetry, circles – RBS, up triangles – NRA, down triangles – SEM). The two dashed lines depict the cubic kinetics ($t^{1/3}$ dependence) for gravimetry and SEM, as well as for NRA and RBS.

For a better overview we plotted the thickness values as a function of oxidation time in Fig. 4. Though different methods give different oxide thickness values the course of each curve is remarkably similar; all of them show the same trend at intermediate time scales. The 40 day sample has a very large oxide thickness, the reason for which is most probably due to the finite number of samples used in our experiments.

The curves show the well-known features of the oxidation kinetics of zirconium alloys. The thickness of the Zircaloy-4 oxide phase increases linearly in the time range of our experiment. This suggests that the samples were in the post-transition range [1], where the corrosion rate is constant, though the number of data points is too small to determine a critical time for the kinetic transition.

For the Zr–1% Nb cubic kinetics is known to prevail (see e.g. [1]). Although the limited number of our data points does not allow a quantitative analysis, it is shown in Fig. 4 that the $t^{1/3}$ dependence (a dotted line for gravimetry and SEM and another one for NRA and RBS) can describe the kinetics quite well. In agreement with the literature [2], no transition between cubic and linear kinetics can be observed in this case.

### 3.3. Electrochemical impedance spectroscopy

We performed a series of electrochemical measurements to characterise the oxide layers. Here we summarise the experiments and results of our OCP and EIS measurements on the samples.

OCP measurements showed that in de-aerated solutions the potential stabilises in a couple of hours and remains constant thereafter. Repeated experiments gave identical results with a reproducibility of about 10 mV. We found that once the OCP became stabilised there exists a wide potential range where the measured electrochemical impedance spectra are very similar to each other. Potentiostatic EIS measurements also show that impedance spectra do not depend on the electrode potential – this implies that it is possible to perform EIS measurements in a wide potential range without measuring the OCP provided that the solution is de-aerated and the electrode is kept on OCP or some chosen potential for a sufficiently long time. With this background we performed a series of EIS measurements on autoclave oxidised Zr–1% Nb samples. As can be seen in Fig. 5, the spectra are related to the constant phase element (CPE) – an impedance, $Z_{\mathrm{CPE}}(\omega) = (1/\sigma)(\mathrm{i}\omega)^{-\alpha}$, where $\sigma$ and $\alpha$ are the CPE coefficient and exponent, respectively, $\omega$ is the angular frequency and i is the imaginary unit (note that for ideal capacitance $\alpha = 1$). We fit the parameters of the $R_s$–(CPE$\|R_p$) equivalent circuit to the measured data where $R_s$ is the solution resistance and $R_p$ is the charge transfer resistance. The CPE parameters are plotted in Fig. 6 as a function of the layer thickness. It can be seen that the CPE coefficients decrease with increasing layer thickness and the CPE exponents show some tendency to approach unity with increasing thickness.

We can interpret the decrease of the CPE coefficient by assuming that the layer behaves as a dielectrics (though the exponent around 0.9 indicates that it has some lossy character). Approximating the CPE by a capacitance $C \approx \sigma$, and using the $C = \varepsilon\varepsilon_0 A/d$ equation we can estimate the layer thickness, $d$. Using a relative permittivity $\varepsilon = 22$ – the relative permittivity of $ZrO_2$

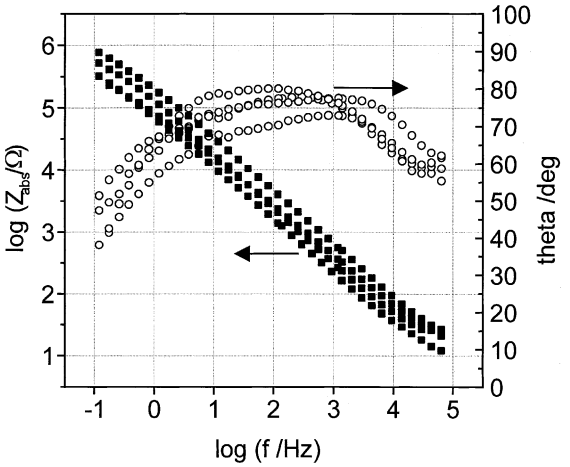


Fig. 5. Typical impedance spectra, measured on Zr–1% Nb samples in 0.05 M $H_2SO_4$ solution (squares – magnitudes, circles – phase angles). We plotted the spectra after subtracting the values of solution resistance.

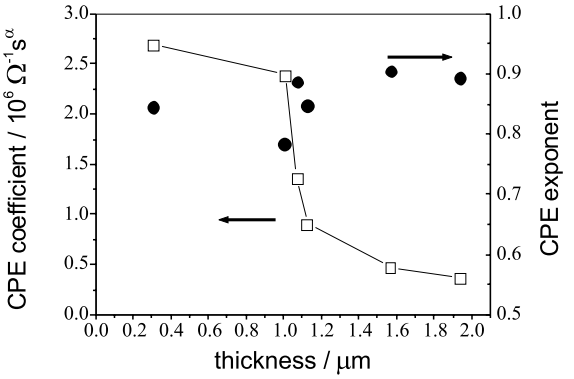


Fig. 6. Zr–1% Nb CPE parameters as a function of oxide layer thickness determined by gravimetry (squares – CPE coefficients, circles – CPE exponents).

varies between 20 and 31.5 in the literature (see. e.g. [2] and references therein) – we obtained thickness values in the order of magnitude of 0.1 μm, i.e., about one order of magnitude smaller than the thickness obtained by the other methods. Our results are in contrast with literature findings stating that the oxide layer thickness can readily be calculated from the CPE coefficient. We should probably also take the porosity of the layers and the double layer capacitance into account when calculating the exact oxide layer thickness. If, however, a space charge layer forms within the oxide, the thickness cannot be calculated directly. The shape of EIS spectra, however, does not allow us to perform a more detailed analysis.

## 4. Summary and conclusions

We have applied five different techniques to characterise oxide layers grown on zirconium alloys in high temperature aqueous solutions all of which are capable of characterising the layer thickness. Gravimetry, electron microscopy, RBS and NRA give approximately the same thickness values.

We have compared the oxide layer growth rates of Zircaloy-4 and Zr–1% Nb, and found that within the limits of uncertainty they are by and large the same. This is so even if the RBS results suggest that the oxide layer of Zr–1% Nb is somewhat thicker in this time range. The kinetics of oxide growth processes was found to obey the laws given in the literature.

The oxide layer formed on Zr–1% Nb is not homogeneous: the surface oxygen content is larger than is expected from the stoichiometric composition of $ZrO_2$. Penetrating deeper into the oxide layer, it can be seen that the zirconium content is almost constant in the $ZrO_2$ phase. The thickness of this phase increases with oxidation time. Further towards the bulk of the sample the oxygen content decreases linearly in an α-Zr(O) phase. The thickness of this phase also increases with oxidation time. A considerable amount of oxygen is dissolved in the metallic alloy phase in the range of 10 μm below the oxide layer.

The thickness values obtained from EIS are much smaller than those from other methods. Though there is a monotonic function connection between the thickness and the CPE exponent, these data are not directly applicable for estimating thicknesses. However, as this is the only in situ method for characterising the oxide layer we shall continue our EIS studies.

## Acknowledgements

One of the authors (G.N.) is indebted to the Hungarian Academy of Sciences for the Bolyai fellowship. Financial support from the National Foundation for Scientific Research, Hungary under contract no. T029894 is acknowledged.

## References

[1] Corrosion of zirconium alloys in nuclear power plants, IAEA-TECDOC-684, 1993.
[2] Waterside corrosion of zirconium alloys in nuclear power plants, IAEA-TECDOC-996, 1998.
[3] Influence of water chemistry on fuel cladding behaviour, IAEA-TECDOC-927, 1997.
[4] WWER reactor fuel performance, modelling and experimental support, in: D. Elenkov, S. Stefanova, I.G. Kolev (Eds.), Proceedings of the Second International Seminar, Sandanski, Bulgaria, April 21–25, 1997, p. 21.
[5] D.I. Schrire, J.H. Pearce, in: A.M. Grade, E.M. Bradley (Eds.), Zirconium in the Nuclear Industry: Tenth International Symposium, ASTM STP 1245, ASTM, 1994, p. 98.
[6] B. Hutchinson, B. Lehtinen, J. Nucl. Mater. 217 (1994) 243.
[7] H.-J. Beie, A. Mitwalsky, F. Garzarolli, H. Ruhmann, H.-J. Sell, in: A.M. Grade, E.M. Bradley (Eds.), Zirconium in the Nuclear Industry: Tenth International Symposium, ASTM STP 1245, ASTM, 1994, p. 615.
[8] G. Wikmark, P. Rudling, B. Lehtinen, B. Hutchinson, A. Oscarsson, E. Ahlberg, in: E.R. Bradley, G.P. Sabol (Eds.), Zirconium in the Nuclear Industry: Eleventh International Symposium, ASTM STP 1295, ASTM, 1996, p. 55.
[9] H. Göhr, J. Schaller, H. Ruhmann, F. Garzarolli, in: E.R. Bradley, G.P. Sabol (Eds.), Zirconium in the Nuclear Industry: Eleventh International Symposium, ASTM STP 1295, ASTM, 1996, p. 181.
[10] H. Göhr, J. Schaller, C.-A. Schiller, Electrochim. Acta 44 (1993) 1961.

[11] J.A. Bardwell, M.C.H- McKubre, Electrochim. Acta 36 (1991) 647.
[12] O. Gebhardt, J. Nucl. Mater. 203 (1993) 17.
[13] J. Krysa, ACH Models Chem. 137 (2000) 249.
[14] J.R. Tesmer, M. Nastasi (Eds.), Handbook of Modern Ion Beam Materials Analysis, MRS, Pittsburgh, PA, USA, 1995.